International Journal of Control and Automation
Vol. 9, No. 4 (2016), pp. 81-94
http://dx.doi.org/10.14257/ijca.2016.9.4.09

Research on Harmonic Suppressing Theory of Magnetic Controlled Reactor Based on Extension Triangle Structure

Wang Jun, Nie Dexin, Chen Feng, Zheng Hao, Tian Cuihua and Zhang Chenmeng*

School of Electrical Engineering, Wuhan University, Wuhan, China
State Grid Electric Power Research Institute, Wuhan, China
State Grid Anhui Electric Power Company, Hefei, China
State Grid Anhui Electric Power Company, Hefei, China
School of Electrical Engineering, Wuhan University, Wuhan, China
School of Electrical Engineering, Wuhan University, Wuhan, China
zhangchenmeng@126.com

Abstract

Magnetic controlled reactor (MCR) is a novel reactive power compensation device. MCR can supply continuous reactive power. But harmonic current is usually generated by MCR. The principle of harmonic current generation of MCR is analyzed in this paper. And then a method based on extension triangle structure MCR is proposed to suppress the particular order harmonic current. An additional winding is connected in series with the three phase windings. In the proposed method, no additional filters are needed and the control method is simple. At last, simulation is done to verify the correctness of this method.

Keywords: *MCR, Harmonic suppression, Extension triangle structure*

1. Introduction

Magnetic controlled reactor (MCR) is a novel dynamic reactive power compensation device, which has the characteristics of flexible adjustment, high overload capacity and high reliability. It draws more and more attentions [1-6]. Single-phase MCR is widely used in electrical railway power quality compensation [7-9] and arc suppression coil [10]. Three-phase MCR is used in machine soft start [11-13], voltage stability of electrical system [14, 15], reactive power compensation and power frequency overvoltage suppression [16, 17]. MCR has a good compensation performance but it will generate harmonic currents. So it's meaningful to make a research on the harmonic characteristics and suppressing harmonics method.

The harmonic currents suppression theory of MCR has become the hotspot nowadays. In [18], two sets of MCRs are parallel connected to suppress the 3^{rd} harmonic current. The theory is making the two MCRs generate 3^{rd} harmonic currents with the same amplitude and opposite phase. In this way, the harmonics of single-phase MCR is conducted. This method needs two MCRs appropriate control and a lot of analog and digital signals should be processed, so the control system design is complex. Additionally, the construction cost is expensive, and the size is inconvenient for indoor installation. A two-stage magnetic controlled reactor (TSMCR) is proposed in [19-20]. The magnetic valve in TSMCR is consisted of two stages with the same length and different area, which is denoted as Stage 1 with smaller area and Stage 2 with a bigger area. When there is no DC magnetic bias under the nominal voltage, Stage 1 is critical saturated. The stage 1 become

ISSN: 2005-4297 IJCA

saturated when there is any DC magnetic bias. Stage 2 is non-saturated at first and when the DC bias is getting bigger, the Stage 2 getting saturated, too. The 3rd harmonic current generated by Stage 1 and Stage 2 is the same amplitude with opposite phase. In this way, the 3rd harmonic current is suppressed. TSMCR will deduce the harmonics of MCR when both the valve stages are saturated, but this method is not effective when Stage 2 is non-saturated. The TSMCR will have more harmonic content when the output capacity is small. So the output capacity range is limited. The length and area of the magnetic valve is optimized in [6] to suppress the harmonics when the output voltage is small. A kind of multi-stage MCR is proposed in [21].

An extension triangle structure three-phase MCR is proposed in this paper. The harmonic generation mechanism is studied firstly. And then an extension triangle structure is proposed and the harmonic suppression mechanism is analyzed. At last, the effectiveness of the proposed method is verified by the simulations.

2. Model of MCR

MCR is an adjustable reactive power compensation device which is based on the core magnetic saturation principle. The structure of MCR is shown in Figure 1. The core is divided into two cores. Each core has a small area section. Four wings are winded symmetrically. Each wind has a tap and the tap ratio is δ. The thyristors K1 and K2 is connected across the taps of one core.

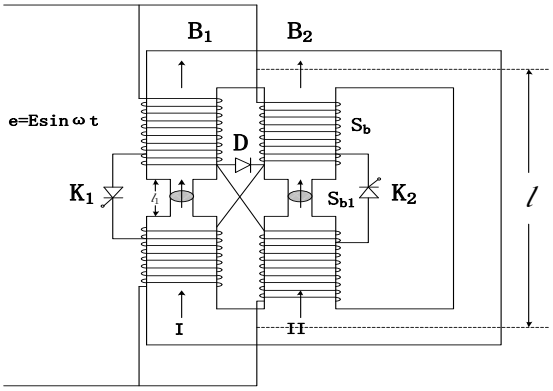

Figure 1. Structure of MCR

The MCR can be regarded as a transformer when K1 and K2 are turn off. The output current is almost 0. At the positive half cycle of *e*, if the thyristor K1 turns on, there will be a DC exciting current ($i_k^{'}$, $i_k^{''}$) which will saturate the small area section. This will increase the output current of MCR. The equivalent circuit when K1 is on is shown in Figure 2(a). The equivalent circuit when K1 is on is shown in Figure 2(b). İt can be obversed that the current direction keeps the same which can be equivalent as a direct current. By changing the value of the operating trigger angle, the value of the exciting current can be changed.

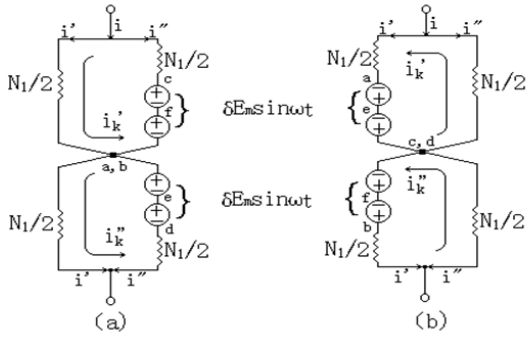

Figure 2. The Equivalent Circuit when Thyristor K1 Or K2 is Turn-On

The equivalent circuit of MCR is shown in Figure 3.

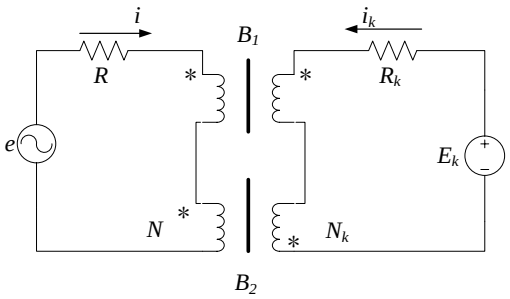

Figure 3. Equivalent Circuit of MCR

In Figure 3, e is the source voltage. E_k is the DC control voltage. i_k is the control current. N is the turns number of working coil and N_k is the turns number of control coil.

According to the Ampere circuit law,

$$\begin{cases} Ni + N_k i_k = l \cdot f(B_1) \\ Ni - N_k i_k = l \cdot f(B_2) \end{cases} \tag{1}$$

In (1), l is the magnetic saturation core length. $f(B)$ is the core magnetization characteristic. B_1 and B_2 are the magnetic induction intensity in iron core 1 and 2, respectively.

It can be conducted that,

$$i = \frac{l}{2N}\left(f(B_1) + f(B_2)\right) \tag{2}$$

Ignore the resistor of the working coil, the waveform of B_1 and B_2 is the superposition of a DC current and AC sine waveform. The waveform of the magnetic induction intensity is shown in Figure 4. B_0 is the DC component of magnetic induction intensity and B_S is the saturated magnetic induction intensity. The AC component of magnetic induction intensity is $B_m \cos(\omega t)$. β represents the saturation degree when the total magnetic induction intensity is over the B_S. Assume the magnetic induction intensity of core 1 and 2 are $B_1 = B_0 - B_m \cos\omega t$ and $B_2 = -B_0 - B_m \cos(\omega t + \pi)$, respectively. The saturation degree is β. The output current of MCR is,

When $0 \le \beta < \pi$,

$$\begin{cases} i = \dfrac{B_m l}{2N\mu_0}\left(-\cos\omega t + \cos\dfrac{\beta}{2}\right) & 0 \le \omega t < \dfrac{\beta}{2} \\ i = 0 & \dfrac{\beta}{2} \le \omega t < \pi - \dfrac{\beta}{2} \\ i = \dfrac{-B_m l}{2N\mu_0}\left(\cos\omega t + \cos\dfrac{\beta}{2}\right) & \pi - \dfrac{\beta}{2} \le \omega t < \pi + \dfrac{\beta}{2} \\ i = 0 & \pi + \dfrac{\beta}{2} \le \omega t < 2\pi - \dfrac{\beta}{2} \\ i = \dfrac{B_m l}{2N\mu_0}\left(-\cos\omega t + \cos\dfrac{\beta}{2}\right) & 2\pi - \dfrac{\beta}{2} \le \omega t < 2\pi \end{cases} \quad (3)$$

When $\pi \le \beta \le 2\pi$

$$\begin{cases} i = \dfrac{B_m l}{2N\mu_0}\left(-\cos\omega t + \cos\dfrac{\beta}{2}\right) & 0 \le \omega t < \pi - \dfrac{\beta}{2} \\ i = \dfrac{-B_m l}{2N\mu_0}\cos\omega t & \pi - \dfrac{\beta}{2} \le \omega t < \dfrac{\beta}{2} \\ i = \dfrac{-B_m l}{2N\mu_0}\left(\cos\omega t + \cos\dfrac{\beta}{2}\right) & \dfrac{\beta}{2} \le \omega t < 2\pi - \dfrac{\beta}{2} \\ i = \dfrac{-B_m l}{2N\mu_0}\cos\omega t & 2\pi - \dfrac{\beta}{2} \le \omega t < \pi + \dfrac{\beta}{2} \\ i = \dfrac{B_m l}{2N\mu_0}\left(-\cos\omega t + \cos\dfrac{\beta}{2}\right) & \pi + \dfrac{\beta}{2} \le \omega t < 2\pi \end{cases} \quad (4)$$

In (3) and (4), $\beta = 2\cos^{-1}\left(\dfrac{B_S - B_0}{B_S}\right)$.

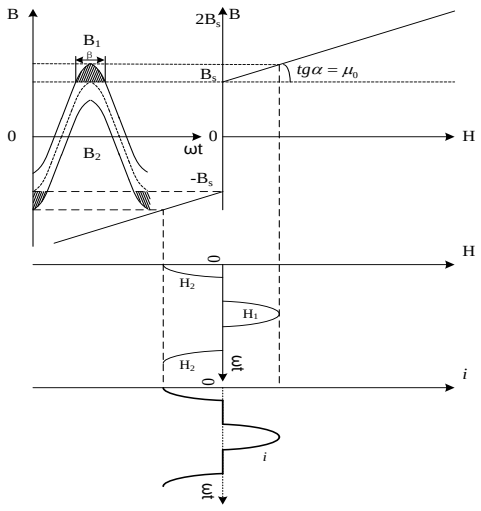

Figure 4. Relationship between Flux Density and Magnetic Intensity

The output current under different β is shown in Figure 5. As it's shown in Figure 5, the amplitude of harmonic currents is varying according to the output current.

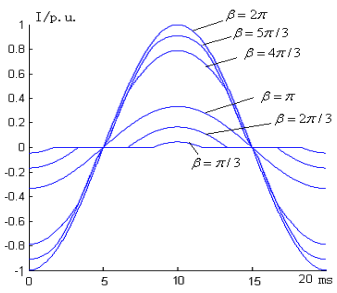

Figure 5. Current Waveforms of MCR under Different B

Make Fourier decomposition to (3) and (4),

$$I_1^* = \frac{1}{2\pi}(\beta - \sin\beta) \tag{5}$$

$$I_{2n+1}^* = \frac{1}{2\pi(2n+1)}\left(\frac{\sin(n\beta)}{n} - \frac{\sin((n+1)\beta)}{n+1}\right) \quad (n = 1, 2, 3, \cdots) \tag{6}$$

According to (5), $I_1^* = 1.0$ when $\beta = 2\pi$. Hence the base value in (6) is the fundamental current amplitude value when the MCR is fully saturated. The 3rd, 5th and 7th harmonic current is shown in Figure 6. The abscissa is the p.u. value of saturated degree β and the ordinate is the p.u. value of harmonic currents. It can be observed in Figure 6 that the nth order harmonic component has n zero point and (n-1) extreme point. The extreme points are symmetrical to and close to the $\beta = \pi$. According to (6), the maximum value of the harmonics when $0 \le \beta \le 2\pi$ is,

$$I_{(2n+1)\max}^* = \frac{2}{\left[(2n-1)^2 - 1\right]\pi} \cdot \sin\left(\frac{n+1}{2n+1}\pi\right) \tag{7}$$

When a MCR is designed, the rated saturated degree $\beta=\beta_n$ of MCR can be flexible selection. But the harmonics at different β_n is widely divergent.

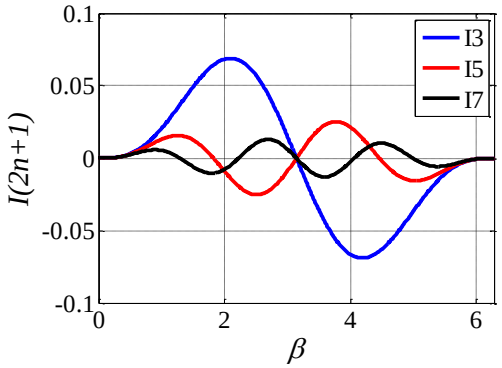

Figure 6. Harmonic Distribution of MCR

In the traditional MCR design method. The rated magnetic saturated degree is designed quite low, which will results in the increase of the harmonics generated by MCR. MCR will have a better harmonic performance when the saturated degree is in π~2π. But the overload capacity is limited. So the rated saturated degree is designed according to the working condition. According to (4), the rated fundamental current related to the extreme current is,

$$I_{1m}^{*} = \frac{1}{2\pi}(\beta_n - \sin\beta_n) \tag{8}$$

If this MCR is used for suppress the switching overvoltage, $I_{1m}^{*} = 1/10$. The rated saturated degree is $\beta_n \approx 92^{\circ}$. The 3rd , 5th, 7th and 11th harmonic currents related to the rated fundamental current is 50%, 17%, 8%, 3.5% according to (4), respectively.

3. Harmonic Currents Suppressing Method based on Extension Triangle Structure

The structure of MCR with extension triangle structure is shown in Figure 7. The structure of three-phase MCR is five-iron-core structure. The control coil is connected by triangle structure. The control structure is extended to the three-phase AC working coils. N_1 is the turns of working coil and N_2 is the turns of control coil. The main flux is

$$\begin{cases} \Phi_a = A_b(B_{11} + B_{12}) \\ \Phi_b = A_b(B_{21} + B_{22}) \\ \Phi_c = A_b(B_{31} + B_{32}) \end{cases} \tag{9}$$

$$\begin{cases} \Phi_a' = A_b(B_{41} + B_{42}) \\ \Phi_b' = A_b(B_{51} + B_{52}) \\ \Phi_c' = A_b(B_{61} + B_{62}) \end{cases} \tag{10}$$

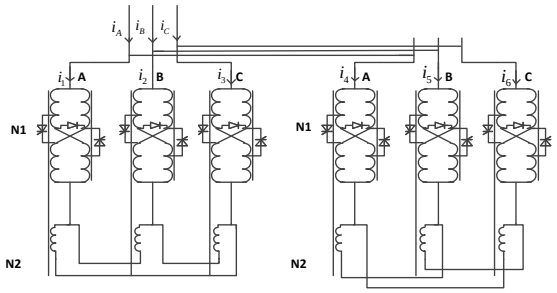

Figure 7. Structure of Three-Phase MCR with Extension Triangle Structure

Since the DC flux is close in the iron core, the control coil is ignored in the analysis of harmonic suppression method. The simplified structure of three-phase MCR with extension triangle structure is shown in Figure 8.

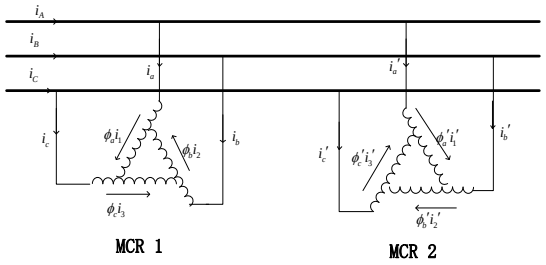

Figure 8. Simplified Graph of Extension Triangle Structure MCR

Assume the three-phase voltage is symmetrical.

$$\begin{cases} u_a = U_m \sin \omega t \\ u_b = U_m \sin(\omega t - \frac{2}{3}\pi) \\ u_c = U_m \sin(\omega t + \frac{2}{3}\pi) \end{cases} \tag{11}$$

The corresponding phasors are

$$\begin{cases} \dot{U}_a = U_m \angle 0° \\ \dot{U}_b = U_m \angle (-\frac{2}{3}\pi) \\ \dot{U}_c = U_m \angle \frac{2}{3}\pi \end{cases} \tag{12}$$

For the MCR 1,

$$\begin{cases} u_a - u_b = N_1 \frac{d\Phi_a}{dt} - (N_1 + N_2)\frac{d\Phi_b}{dt} \\ u_b - u_c = N_1 \frac{d\Phi_b}{dt} - (N_1 + N_2)\frac{d\Phi_c}{dt} \\ u_c - u_a = N_1 \frac{d\Phi_c}{dt} - (N_1 + N_2)\frac{d\Phi_a}{dt} \end{cases} \tag{13}$$

According to (8),

$$\begin{bmatrix} 1 & -1 & 0 \\ 0 & 1 & -1 \\ -1 & 0 & 1 \end{bmatrix} \begin{bmatrix} \dot{U}_a \\ \dot{U}_b \\ \dot{U}_c \end{bmatrix} = j\omega(N_1 + N_2) \begin{bmatrix} \alpha & -1 & 0 \\ 0 & \alpha & -1 \\ -1 & 0 & \alpha \end{bmatrix} \begin{bmatrix} \dot{\Phi}_a \\ \dot{\Phi}_b \\ \dot{\Phi}_c \end{bmatrix} \tag{14}$$

In (13), $\alpha=N_1/(N_1+N_2)$. It can be conducted that,

$$\begin{bmatrix} \dot{\Phi}_a \\ \dot{\Phi}_b \\ \dot{\Phi}_c \end{bmatrix} = \frac{1}{j\omega(N_1 + N_2)} \begin{bmatrix} \alpha & -1 & 0 \\ 0 & \alpha & -1 \\ -1 & 0 & \alpha \end{bmatrix}^{-1} \begin{bmatrix} 1 & -1 & 0 \\ 0 & 1 & -1 \\ -1 & 0 & 1 \end{bmatrix} \begin{bmatrix} \dot{U}_a \\ \dot{U}_b \\ \dot{U}_c \end{bmatrix} \tag{15}$$

From (7) and (10),

$$\begin{bmatrix} \dot{\Phi}_a \\ \dot{\Phi}_b \\ \dot{\Phi}_c \end{bmatrix} = \frac{\sqrt{3}U_m}{\omega(N_1 + N_2)(\alpha^2 + \alpha + 1)} \begin{bmatrix} \angle(-\gamma - \frac{\pi}{2}) \\ \angle(-\gamma - \frac{\pi}{2} - \frac{2\pi}{3}) \\ \angle(-\gamma - \frac{\pi}{2} + \frac{2\pi}{3}) \end{bmatrix} \tag{16}$$

In (15), $\gamma = tg^{-1}\frac{1-\alpha}{\sqrt{3}(1+\alpha)}$.

As it's shown in (11), the phase relationship between the working main flux and the source voltage can be adjusted by the turn ratio between the main coil and the

control coil.

The flux phasor of MCR 2 can be obtained similarly.

$$\begin{bmatrix} \dot{\Phi}_a' \\ \dot{\Phi}_b' \\ \dot{\Phi}_c' \end{bmatrix} = \frac{\sqrt{3}U_m}{\omega(N_1+N_2)(\alpha^2+\alpha+1)} \begin{bmatrix} \angle(\gamma-\frac{\pi}{2}) \\ \angle(\gamma-\frac{\pi}{2}-\frac{2\pi}{3}) \\ \angle(\gamma-\frac{\pi}{2}+\frac{2\pi}{3}) \end{bmatrix} \tag{17}$$

According to (15) and (16), the phase difference of the main flux of MCR 1 and 2 is 2γ.

The magnetic field intensity $H_a(t)$、$H_b(t)$、$H_c(t)$ in MCR 1 is

$$\begin{bmatrix} H_a(t) \\ H_b(t) \\ H_c(t) \end{bmatrix} = \begin{bmatrix} \sum_{k=1}^{\infty} H_{(6k\pm1)m} \sin[(6k\pm1)(\omega t-\frac{\pi}{2}-\gamma)+\theta_{FK}] \\ \sum_{k=1}^{\infty} H_{(6k\pm1)m} \sin[(6k\pm1)(\omega t-\frac{\pi}{2}-\gamma-\frac{2\pi}{3})+\theta_{FK}] \\ \sum_{k=1}^{\infty} H_{(6k\pm1)m} \sin[(6k\pm1)(\omega t-\frac{\pi}{2}-\gamma+\frac{2\pi}{3})+\theta_{FK}] \end{bmatrix} \tag{18}$$

In (17), θ_{FK} is the iron loss angle.

Similarly, the magnetic field intensity $H'_a(t)$、$H'_b(t)$、$H'_c(t)$ in MCR 2 is

$$\begin{bmatrix} H_a'(t) \\ H_b'(t) \\ H_c'(t) \end{bmatrix} = \begin{bmatrix} \sum_{k=1}^{\infty} H_{(6k\pm1)m} \sin[(6k\pm1)(\omega t-\frac{\pi}{2}+\gamma)+\theta_{FK}] \\ \sum_{k=1}^{\infty} H_{(6k\pm1)m} \sin[(6k\pm1)(\omega t-\frac{\pi}{2}+\gamma-\frac{2\pi}{3})+\theta_{FK}] \\ \sum_{k=1}^{\infty} H_{(6k\pm1)m} \sin[(6k\pm1)(\omega t-\frac{\pi}{2}+\gamma+\frac{2\pi}{3})+\theta_{FK}] \end{bmatrix} \tag{19}$$

In Figure 8, the node current equation is

$$\begin{cases} i_1-i_2=i_a \\ i_2-i_3=i_b \\ i_3-i_1=i_c \\ i_1'-i_3'=i_a' \\ i_2'-i_1'=i_b' \\ i_3'-i_2'=i_c' \end{cases} \tag{20}$$

The corresponding magnetic potential is

$$\begin{cases} i_aN_1+i_1N_2=H_a(t)l \\ i_bN_1+i_2N_2=H_b(t)l \\ i_cN_1+i_3N_2=H_c(t)l \\ i_a'N_1+i_1'N_2=H_a'(t)l \\ i_b'N_1+i_2'N_2=H_b'(t)l \\ i_c'N_1+i_3'N_2=H_c'(t)l \end{cases} \tag{21}$$

l is the length of magnetic loop.

Substitute (19) and (20) into (17) and (18),

$$\begin{cases} \begin{bmatrix} i_a(t) \\ i_b(t) \\ i_c(t) \end{bmatrix} = \dfrac{\sqrt{3}l}{(N_1+N_2)\sqrt{\alpha^2+\alpha+1}} \\ \qquad \begin{bmatrix} \sum_{k=1}^{\infty} H_{(6k\pm1)m} \sin[(6k\pm1)(\omega t-\frac{\pi}{2})-6k\gamma+\theta_{FK}] \\ \sum_{k=1}^{\infty} H_{(6k\pm1)m} \sin[(6k\pm1)(\omega t-\frac{\pi}{2})-6k\gamma+\theta_{FK}\mp\frac{2\pi}{3}] \\ \sum_{k=1}^{\infty} H_{(6k\pm1)m} \sin[(6k\pm1)(\omega t-\frac{\pi}{2})-6k\gamma+\theta_{FK}\pm\frac{2\pi}{3}] \end{bmatrix} \\ \begin{bmatrix} i_a'(t) \\ i_b'(t) \\ i_c'(t) \end{bmatrix} = \dfrac{\sqrt{3}l}{(N_1+N_2)\sqrt{\alpha^2+\alpha+1}} \\ \qquad \begin{bmatrix} \sum_{k=1}^{\infty} H_{(6k\pm1)m} \sin[(6k\pm1)(\omega t-\frac{\pi}{2})+6k\gamma+\theta_{FK}] \\ \sum_{k=1}^{\infty} H_{(6k\pm1)m} \sin[(6k\pm1)(\omega t-\frac{\pi}{2})+6k\gamma+\theta_{FK}\mp\frac{2\pi}{3}] \\ \sum_{k=1}^{\infty} H_{(6k\pm1)m} \sin[(6k\pm1)(\omega t-\frac{\pi}{2})+6k\gamma+\theta_{FK}\pm\frac{2\pi}{3}] \end{bmatrix} \end{cases} \tag{22}$$

In (21), the phase difference between the same phase of MCR 1 and 2 current is $2\times 6k\gamma$ (k=1,2,3,$\cdots$). To eliminate 5th and 7th harmonics, the phase difference should be 180°.

$$2\times 6k\gamma = \pm 180° \quad (\text{k=1}) \tag{23}$$

It can be conducted that γ=15°. So if two MCRs with γ=15° parallel connected, n=6$k\pm$1 (k is odd) order harmonic current will not injected into the grid.

A practical calculation example is shown below. Assume the saturated degree of MCR is 75°. The *a*-phase output current with and without external triangle structure is shown in Figure 9. It can be observed that there are more harmonic currents without the external triangle structure.

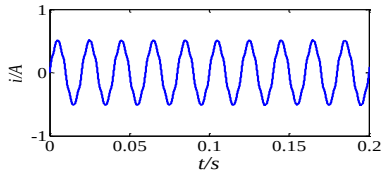

(a)

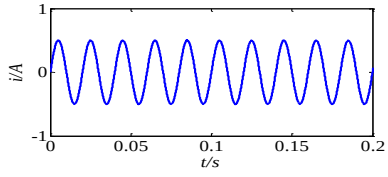

(b)

Figure 9. Comparing of Output Current With and Without External Triangle Structure. (A) Without External Triangle Structure. (B) With External Triangle Structure

4. Simulation Results

To verify the effectiveness of the proposed structure, simulation is done by MATLAB/Simulink. The simulation structure is shown in Figure 7. The rated voltage of MCR is 35kV. The phase angle difference is 30° to eliminate 5th and 7th harmonic currents.

Two working conditions are simulated to verify the proposed structure. The saturate degree is 70° and 50°, respectively.

1) β=70°

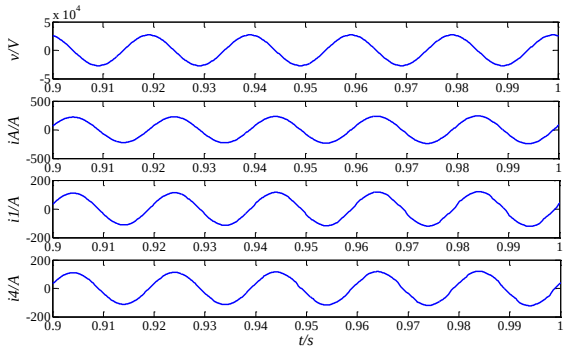

Figure 10. Simulation Result (β=70°)

The simulation results at this working condition are shown in Figure 10. In Figure 10, from top to bottom are the grid voltage, total output current, output current of MCR 1 and output current of MCR 2. It can be observed that the total output current is better than the single output current of one MCR.

To make a clear comparison, FFT is done for the currents above. The analysis results are shown in Figure 11. It can be observed the 5th and 7th harmonic current is significantly deduced. The THD is only 1.48%. While the 5^{th} and 7^{th} harmonic currents content in single MCR is not eliminated. The THDs are 5.18% and 5.03%, respectively.

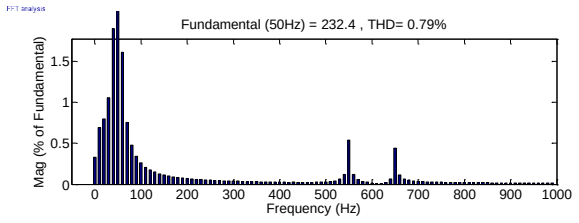

(a)

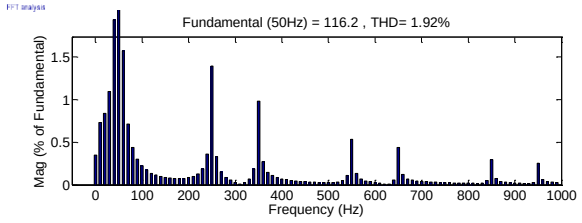

(b)

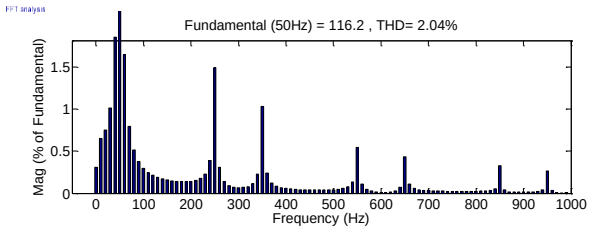

(c)

Figure 11. Frequency Spectrum of Output Current. (a) FFT Analysis of Total Output Current. (b) FFT Analysis of MCR 1. (c) FFT Analysis of MCR 2. (β=70°)

The comparison of total output current, current of MCR 1 and MCR 2 is shown in Table 1. It can be observed that the 5th and 7th harmonic currents are decreased. The 3rd and 9th harmonic currents are almost stay the same because there is a 3rd harmonic loop in the external triangle structure.

Table 1. Comparison of Output Currents (β=70°)

	THD%	3rd %	5th %	7th %	9th %
Total	1.48	0.17	0.08	0.05	0.04
MCR1	5.18	0.14	4.18	2.66	0.06
MCR2	5.03	0.21	4.03	2.59	0.05

2) β=50°

The simulation results at this working condition are shown in Figure 12. In Figure 12, from top to bottom are the grid voltage, total output current, output current of MCR 1 and output current of MCR 2. It can be observed that the total current i_A is almost sinusoidal while the output current of single MCR (i_1 and i_4) contents harmonic currents.

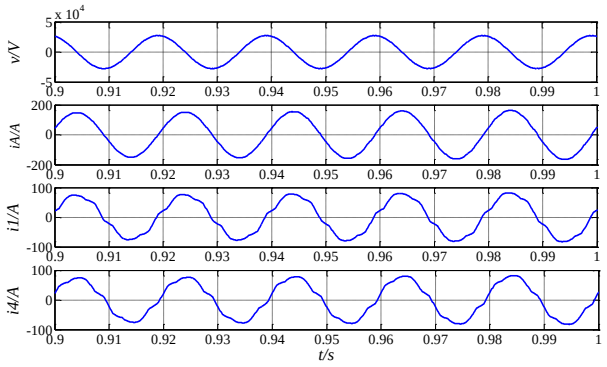

Figure 12. Simulation Result (β=50°)

The FFT analysis is shown in Figure 13. The 5th and 7th harmonics are deduced and the total output current THD is only 1%, while the THD of single MCR is 4% and 5%, respectively.

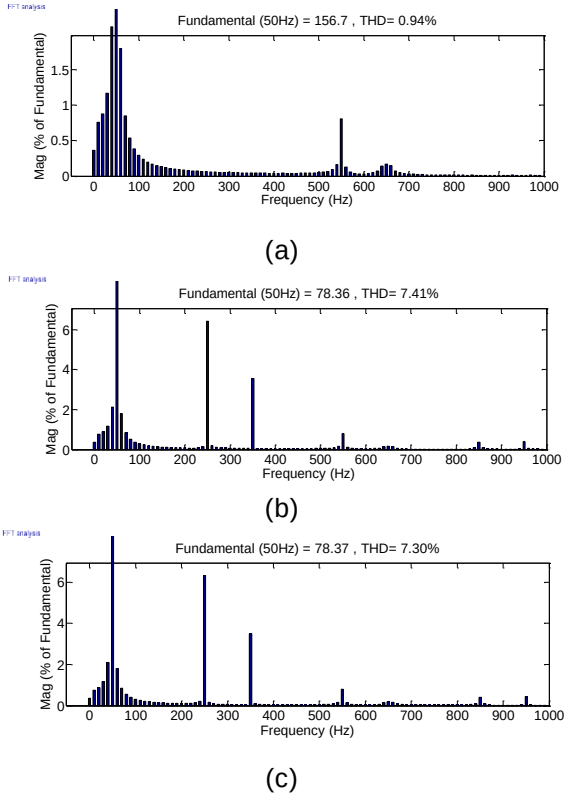

Figure 13. Frequency Spectrum of Output Current. (A) FFT Analysis of Total Output Current. (B) FFT Analysis of MCR 1. (C) FFT Analysis of MCR 2. (B=50°)

The comparison of total output current, current of MCR 1 and MCR 2 when β=50° is shown in Table 2. It can be observed that the 5th and 7th harmonic currents are decreased when the external triangle structure is used.

Table 2. Comparison of Output Currents (B=50°)

	THD%	3rd %	5th %	7th %	9th %
Total	0.94	0.13	0.06	0.04	0.04
MCR1	7.14	0.12	6.42	3.55	0.04
MCR2	7.30	0.14	6.31	3.50	0.04

5. Conclusion

To suppress the harmonics in three-phase MCR, an external triangle structure three-phase MCR is proposed. The principle of harmonic currents generation of MCR is analyzed firstly. And then a novel external triangle structure MCR is proposed. The working principle of proposed MCR is explored and draws the conclusion that two parallel connected MCR with a specific phase angle difference would eliminate the specific harmonic currents. At last, simulation is done to verify the effectiveness of the proposed structure.

References

[1] Z. Deng, X. Wc and F. Zhou, "Modeling of extra-high voltage magnetically controlled shunt reactor", Proceedings of the CSEE, vol. 28, no. 36, **(2008)**.
[2] X. Wang, Z. Deng and K. Yu, "Steady-state characteristics of extra-high voltage magnetically controlled shunt reactor", Proceedings of the CSEE, vol. 28, no. 33, **(2008)**.

[3] M. Tian and Q. Li, "An equivalent circuit and simulation analysis of magnetically-saturated controllable reactors", Transactions of China Electrotechnical Society, vol. 18, no. 6, **(2003)**
[4] M. Tian and Q. Li, "An equivalent physical model and a mathematical model of the controlled saturable reactor [J]", Transactions of China Electrotechnacal Society, vol. 17, no. 4, **(2002)**.
[5] C. Tian and B. Chen, "Application of magnetically controlled reactor in 750kV power system", Transactions of China Electrotechnical Society, vol. 20, no. 1, **(2005)**.
[6] H. Li, H. Liu and Z. Ying, "Control system design based on magnetic controlled reactor", High Voltage Engineering, vol. 40, no. 1, **(2014)**.
[7] J. Yuan, S. Li and C. Zhang, "Research on collaborative compensation of electrified railway's three-phase unbalance load", Transactions of China Electrotechnical Society, vol. 26, no. 1, **(2011)**.
[8] C. Cai, B. Chen and A. Yuan, "Electromagnetic hybrid optimized compensation method of negative sequence for high-speed railway traction supply system", Transactions of China Electrotechnical Society, vol. 28, no. 5, **(2013)**.
[9] C. Baichao, Z. Chenmeng and Y. Ao, "Resaerch on a Hybrid Compensation System for V/V High-speed Railway Power Supply System", Transactions of China Electrotechnical Society, vol. 28, no. 12, **(2013)**.
[10] W. Qian, C. Xu and X. Bo, "Design of key parameters about two-stage magnetic valve arc-suppression coil", Transactions of China Electrotechnical Society, vol. 26, no. 10, **(2011)**.
[11] P. Jing, C. Baichao and Y. Mengze, "Development of Magnetic Saturation Controllable Soft Starter for Motors", Large Electric Machine and Hydraulic Turbine, vol. 25, no. 4, **(2006)**.
[12] D. Shanshan, C. Baichao and Y. Mengze, "Application of Magnetic-valve Type of Controllable Reactor into Soft-start of HV Motors", Electrical Machinery Technology, vol. 22, no. 4, **(2007)**.
[13] Y. Mengze, C. Baichao and H. Qiuping, "The Simulation of Medium-voltage Synchronous Motor Soft Starter Based on Magnetic-valve Controllable Reactor", Large Electric Machine and Hydraulic Turbine, vol. 19, no. 1, **(2008)**.
[14] Y. Mengze, C. Baichao and T. Cuihua, "High voltage static var reactive power compensator using shunt magnetically controllable reactor", High Voltage Engineering, vol. 35, no. 7, **(2009)**.
[15] C. Zhenhu, L. Jiyong and H. Xiangwei, "Design and application of dynamic reactive-load compensation device based on magnetically controlled reactor", Power System Technology, vol. 29, no. 7, **(2005)**.
[16] P. Junzhen, S. Meng and S. Hongchun, "Analysis of the Influence of Saturated Core Superconducting Controllable Reactor on Line Power Frequency Overvoltage", High Voltage Apparatus, vol. 9, no. 20, **(2013)**.
[17] X. Haiying, C. Baichao and Z. Yadi, "UHV switching overvoltage suppression by quick response magnetically controlled reactor", Electric Power Automation Equipment, vol. 29, no. 1, **(2009)**.
[18] C. Baichao, T. Cuihua and L. Baihua, "Principle and implementation of a harmonic depression approach for single-phase controlled saturable reactor', Proceedings of the CSEE, vol. 22, no. 3, **(2002)**.
[19] T. Cuihua and C. Baichao, "Study of low distortion two stages saturable magnetically controlled reactor", Transactions of China Electrotechnical Society, vol. 21, no. 1, **(2006)**.
[20] C. Xuxuan, C. Baichao and T. Cuihua, "Optimization technique of harmonic suppression for TSMCR", Electric Power Automation Equipment, vol. 31, no. 5, **(2011)**.
[21] C. Xuxuan, T. Cuihua and C. Baichao, "Mathematical model for harmonics analysis of the multi-stagesaturable magnetic-valve controllable reactor", Transactions of China Electrotechnical Society, vol. 26, no. 3, **(2011)**.

Author

Wang Jun, he was born in 1964. He is a Ph.D. student of Wuhan University now. His research interest is transportation electrical automation and power grid stability.